

Spectrum evolution and chirping of laser-induced spin wave packets in thin iron films

Ia. A. Filatov,^{1, a)} P. I. Gerevenkov,¹ M. Wang,² A. W. Rushforth,² A. M. Kalashnikova,¹ and N. E. Khokhlov¹

¹⁾*Ioffe Institute, 26 Politekhnicheskaya st., 194021, St. Petersburg, Russian Federation*

²⁾*School of Physics and Astronomy, The University of Nottingham, NG7 2RD Nottingham, UK*

(Dated: 2 November 2021)

We present the experimental study of ultrafast optical excitation of surface magnetostatic spin wave (MSSW) packets and their spectral properties in thin films of pure iron. As the packets leave the excitation area and propagate in space, their spectra evolve non-trivially. Particularly, low or high frequency components are suppressed at the border of the excitation area depending on the orientation of the external magnetic field with respect to the magnetocrystalline anisotropy axes of the film. The effect is ascribed to the ultrafast local heating of the film. Further, the time resolution of the implemented all-optical technique allows us to extract the chirp of the MSSW packet in the time domain via wavelet analysis. The chirp is a result of the group velocity dispersion of the MSSW and, thus, is controlled by the film magnetic parameters, magnetization and anisotropy, and external field orientation. The demonstrated tunable modulation of MSSW wave packets with femtosecond laser pulses may find application in future magnonic-photonic hybrid devices for wave-based data processing.

Developments in neuromorphic computing and pattern recognition largely rely on signal processing, going beyond the schemes offered by conventional electronics. Spin waves (SWs), or coherent magnons, in magnetically ordered structures are considered as a potential alternative to electrons in semiconductor devices for the transmission and processing of information in a special area of spintronics named magnonics¹⁻⁵. The most prominent feature of SWs is the possibility to transfer information about the magnetic moment without electric currents, thereby minimizing ohmic losses. Furthermore, a growing number of works refer to SWs as an effective tool for wave-based logic and calculations⁴⁻⁸. Moreover, SW transport in data processing devices is potentially available at sub-100-nm scales. However, such a small scale for real application components demands appropriate materials with easy-to-manufacture procedures and satisfactory magnonic properties, such as high frequencies of the SWs, their tunability and easy integration into semiconductor electronic circuits. These features are native for transition-metal based micro- and nanometer sized waveguides for SWs, making them promising candidates for nano-magnonic applications^{2,4}. Furthermore, the intrinsic strong anisotropy fields in metal nano-waveguides play the role of an additional knob to design the properties of SWs, such as the SW dispersion and the corresponding phase evolution^{9,10}. The latter is crucial to make SWs effective tools for wave-based logic and interferometric calculations⁴⁻⁸, particularly, in speeding up computationally demanding tasks such as image and speech recognition^{11,12}. The described practical purposes of magnonics require appropriate research tools to excite and inspect the wave nature of SWs. Recently, ultrafast laser pulses were introduced as such tool because

they can excite SW with exceptional tunability^{10,13-18}. However, laser excitation is intrinsically broad-band and inhomogeneous, which has a significant effect on the properties of the generated SW packets, limiting the spatial and temporal profile and leading to large spectral width. Therefore, understanding the propagation of such wave packets is essential for developing applications of optically generated SWs for future magnonic-photonic hybrid devices.

In this letter, we report on the experimental observation of controllable spectrum evolution and frequency modulation of laser-induced magnetostatic surface waves (MSSWs) in thin films of pure iron. We show, that the spectral features of MSSW wave packets can be tuned by choosing the orientation of an external magnetic field with respect to the axes of the magnetocrystalline anisotropy. As the optically excited MSSW packets are broad-band and propagate in a dispersive medium, they obtain a chirp — a time delay between distinct frequency components. We clearly detect the chirping at the μm spatial scale. The findings are crucial for the design of hybrid opto-magnonic wave-based data processing circuits.

Our investigations are carried out using epitaxial films of iron with thicknesses $d = 10$ and 20 nm. The films are deposited on $350\text{-}\mu\text{m}$ thick GaAs (001) substrates by magnetron sputtering and are capped with a 2.5-nm -thick chromium layer for protective purposes. The films possess pronounced cubic and interface-induced uniaxial in-plane magnetic anisotropy similar to other epitaxial thin films of iron and its alloys on GaAs substrates¹⁹⁻²¹.

Excitation and detection of MSSWs are performed using a space-time-resolved magneto-optical Kerr effect (STR-MOKE) pump-probe setup²². Pump and probe laser pulses with central wavelengths of 750 nm and 1050 nm, respectively, a duration of 120 fs, 70 MHz repetition rate, are focused normally onto opposite sides of the iron film into $3.5\text{-}\mu\text{m}$ -diameter spots using microobjectives.

^{a)}yaroslav.filatov@mail.ioffe.ru; <http://www.ioffe.ru/ferrolab/>

The fluence of the pump pulses is of 4.5 mJ/cm^2 , and the probe pulses have a fluence of about 20 times lower. The temporal resolution is achieved with an opto-mechanical delay line placed in the pump path. The spatial scan is realized by placing the pump microobjective on a 2-axes piezo stage. The experiments are done in the Damon-Eshbach configuration, i.e., an external static magnetic field $\mu_0 \mathbf{H} = 100 \text{ mT}$ is applied in the film's plane and the propagation of the MSSW is detected perpendicularly to \mathbf{H} with varying distance between the pump and probe spots on the sample surface. In the sample's plane \mathbf{H} is aligned at different angles with respect to the magnetocrystalline anisotropy axes of the film. The excitation mechanism of the MSSW in the experiments is an ultrafast change of the magnetocrystalline anisotropy caused by ultrafast heating induced by the pump pulse, similar to the recent experiments of MSSW excitation in galfenol ($\text{Fe}_{0.81}\text{Ga}_{0.19}$) films^{10,22}. We investigate propagating MSSWs for two directions of \mathbf{H} : (i) \mathbf{H} is aligned along the sample's hard anisotropy axis and (ii) \mathbf{H} is at 15° with respect to the easy anisotropy axis, referred further as HA- and EA-configurations, respectively.

Figure 1(a) shows the spatial-temporal map of the polar Kerr rotation angle for the probe measured with the STR-MOKE setup in the sample with $d = 10 \text{ nm}$ in

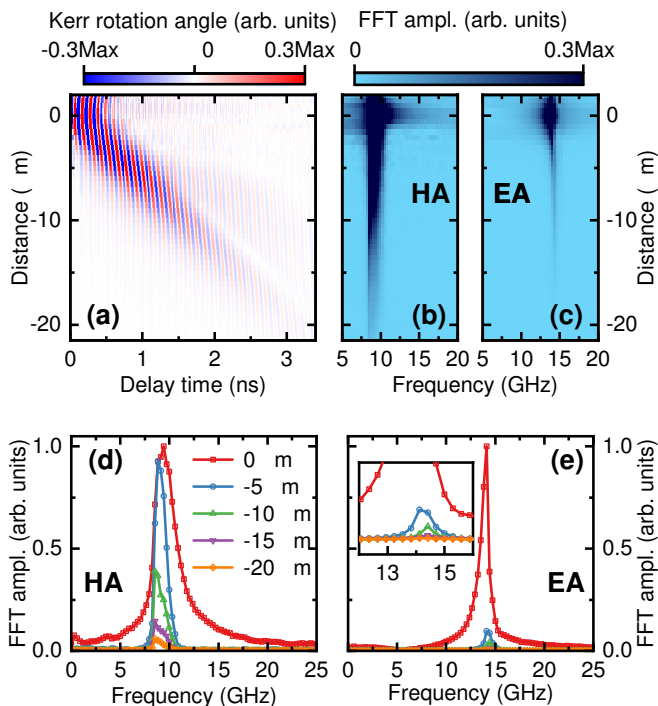


FIG. 1. (a) Polar Kerr signal induced by propagating MSSW packet in the time-space domain for Fe film with $d = 10 \text{ nm}$ in the HA-configuration. (b,c) Space-frequency maps of the packet for the HA- (b) and EA- (c) configurations. (d, e) FFT spectra of the packet at different pump-probe distances for the HA- (d) and EA- (e) configurations. Inset in (e) shows enlarged area of the same spectra.

the HA-configuration. The color bar spans up to 0.3 of the maximum amplitude of the measured Kerr signal to show the propagation of the MSSW packet beyond the distance at which its amplitude decreases by a factor of e . The shape and slope of the phase pattern serves as evidence that the detected Kerr signal originates from the propagating MSSW wave packet. Thus, the propagation of laser-induced MSSW wave packets over a distance of more than $10 \mu\text{m}$ is clearly observed. Such propagation distance is comparable and even larger than that of typical values in other metallic materials used in real magnonic circuits²³.

Next, we analyze the spectral composition of the propagating MSSW wave packet by performing fast Fourier transform (FFT) analysis of signal in the time domain for each pump-probe distance. The result is shown in Fig. 1(b,c) for the 10-nm sample in the HA- and EA-configurations, respectively. The color bar is also set at 0.3 of the maximum amplitude to more clearly characterize the decrease of the MSSW amplitude during propagation. Compression of the spectral width and a shift of the frequency with maximal FFT amplitude are observed during the propagation of the MSSW from the excitation spot. More explicit confirmation of such spectral changes is possible by analyzing the individual spectra at different pump-probe distances (Fig. 1(d,e)). The central frequency of the propagating MSSW shifts to the lower or higher part of the spectrum observed in the excitation area for the HA- and EA-configurations, respectively, in agreement with previous results for galfenol films on GaAs substrates^{10,22}. The observed spectral evolution is associated with different MSSW dispersion relations inside and outside the pump-heated area. Indeed, effective anisotropy fields are partially suppressed by an abrupt decrease of the anisotropy parameters and magnetization inside the excitation area²⁴. This leads to a shift of the MSSW dispersion inside the pump area to the higher or lower frequency range depending on the orientation of \mathbf{H} because of the different manner in which the anisotropy field enters the total effective field: i.e. the effective anisotropy field is subtracted from (added to) \mathbf{H} in the HA-(EA-)configuration, leading to a decrease (increase) of the total effective magnetic field in the sample, which defines the frequency of the MSSW^{25,26}. Since the pump has a limited diameter, it excites a limited band of wavenumbers inside the spot^{13,27}. This sets an upper limit on the spectral range of the excited MSSW frequencies, with the lower limit being the ferromagnetic resonance frequency. MSSWs propagating outside the pump have the same limitation on the wavenumber, but the corresponding frequency range is shifted up (down). This, in turn, sets upper (lower) bounds on the available frequency in the MSSW spectrum. A detailed description of the spectrum evolution of MSSWs in the presence of strong magneto-crystalline anisotropy is given elsewhere^{10,22}.

Using FFT spectra, we determine values of the MSSW propagation length l_p for both magnetic field configura-

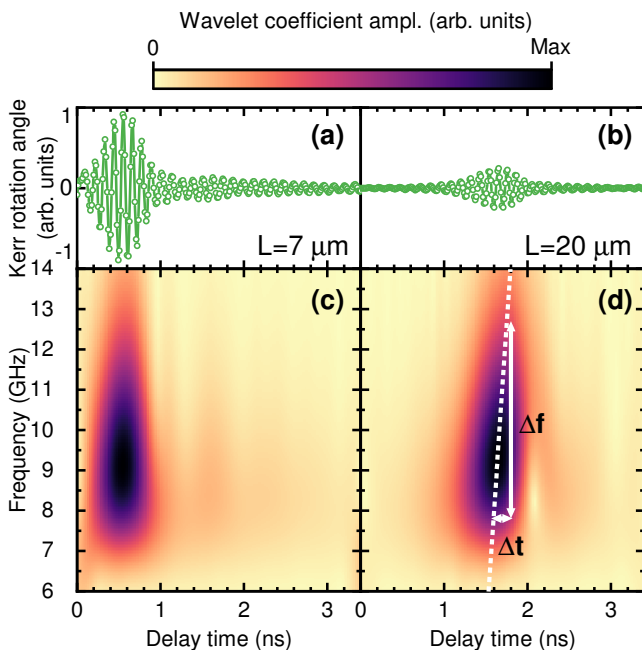


FIG. 2. (a,b) Wave packet signals at distances of 7 and 20 μm from the pump spot in the time domain for the 20-nm film in the HA-configuration. (c,d) Corresponding wavelet spectrograms in the time-frequency domain. Dashed line on (d) shows variation of the frequency peak with time. Double arrows show the variation of the frequency Δf and time shift Δt schematically.

tions by fitting the dependence of the integral of the central peak in the FFT spectra, S on the pump-probe distance, L with the exponential function $S \propto \exp(-L/l_p)$. We determine l_p in the range of $L > 3 \mu\text{m}$, i.e. starting from the edge of the pump area, which represents the value of l_p for the MSSW propagating in the non-heated iron film. The obtained values of l_p for all samples are larger than 6 μm in the HA-configuration and less than 5 μm in the EA-configuration (see Table I). The observation that l_p is larger in the HA-configuration is in good agreement with previous works on MSSWs in cubic anisotropic metal films^{9,10}. The effect is connected with the reduction of the total in-plane effective field in the HA-configuration and is discussed in detail elsewhere⁹.

As shown above, the spectrum of the MSSW becomes strongly asymmetric with distance (Fig. 1(d,e)). Hence, we may expect that the wave packet of the MSSW acquires a phase or frequency modulation, i.e., the frequency components propagate with different velocities resulting in the temporal shift between them. We implement continuous wavelet transform with Morlet mother wavelet similar to opto-acoustic pump-probe experiments^{28,29} to extract information about the frequency evolution in the time domain. Indeed, the resulting analysis reveals the shift of the frequency components f with time t , increasing with L (Fig. 2(c,d)).

To characterise the shift, we approximate the regis-

tered frequency modulation of the MSSW packets with a linear function $f(t) = f_c + \nu t$, where f_c is a central wave packet frequency, $\nu = \frac{\partial f}{\partial t}$ is a parameter characterising the chirp. The non-zero value of ν appears when a wave packet propagates in a dispersive medium, and its group velocity depends on f ³⁰⁻³². The equation for the complex packet's envelope in this case is obtained by expanding the dispersion relation $f(k)$, where k is a wave vector, into a Taylor series upto the derivative of the second order. Importantly, the obtained parabolic partial-derivative equation for the complex envelope has the same form for optical pulses^{31,32} and for magneto-static waves³³ both. The resulting equation for the chirp parameter of a Gaussian wave packet at distance L is^{31,32}:

$$2\pi\nu(L) = \frac{2L}{\beta_2(L^2 + L_D^2)}, \quad (1)$$

where $\beta_2 = \frac{\partial^2 k}{\partial \omega^2}$, $\omega = 2\pi f$, $L_D = T_0^2/|\beta_2|$, and T_0 is an initial half duration of the packet at level e^{-1} .

To compare the chirp described by Eq. (1) with experimental value of ν , we used the analytic dispersion of MSSW in the thin film limit ($kd \ll 1$) and for small wavenumbers (the exchange contribution to the spin wave energy is negligible) in a simplified form^{26,34,35}:

$$f(k) = \left(f_{\text{FMR}}^2 + F^2 \frac{kd}{2} \right)^{1/2}, \quad (2)$$

where f_{FMR} is the ferromagnetic resonance frequency, and F is a constant. Values of f_{FMR} and F are determined by the gyromagnetic ratio, saturation magnetization, and anisotropy parameters of the film, and the mutual orientation of \mathbf{H} and anisotropy axes. Here we obtain f_{FMR} and F by fitting the experimental MSSW dispersion reconstructed from time-space maps via two-dimensional FFT (Fig. 3(a)). The results of the fits are presented in Table I. Equations (1,2) give the result:

$$\nu(L) = \frac{2F^2 dL}{4L^2 + (\pi F^2 d T_0^2)^2}. \quad (3)$$

The calculations of $\nu(L)$ show the same trend with the experimental spectrograms (Fig. 3(b)). Deviation of experiment and analytical Eq. (3) is due to several approximations used to derive Eq. (1). One of them is $\Delta f \ll f_c$, where Δf is the spectral width of the wave packet, which is important for Taylor series approach. The condition is not fully satisfied in the experiments as we detect MSSW packets with $\Delta f \approx 4 \text{ GHz}$ at $f_c \approx 9 \text{ GHz}$ (see Fig. 1(c-e) and Fig. 2(c,d)). Second approximation is that, Eq. (1) is obtained for Gaussian envelope of the packet at the entrance of the media. The experimental envelope of MSSW is visibly asymmetric in the time domain (Fig. 2(a)). Thus, more comprehensive theoretical analysis of the evolution of optically excited SW packets

TABLE I. Parameters of MSSW obtained in experiments

d (nm)	HA-configuration			EA-configuration		
	l_p (μm)	f_{FMR} (GHz)	F (GHz)	l_p (μm)	f_{FMR} (GHz)	F (GHz)
10	6.1 ± 0.1	8.3 ± 0.1	152 ± 4	2.6 ± 0.1	13.9 ± 0.2	220 ± 10
20	8.9 ± 0.3	8.2 ± 0.1	148 ± 5	4.7 ± 0.1	14.9 ± 0.3	150 ± 15

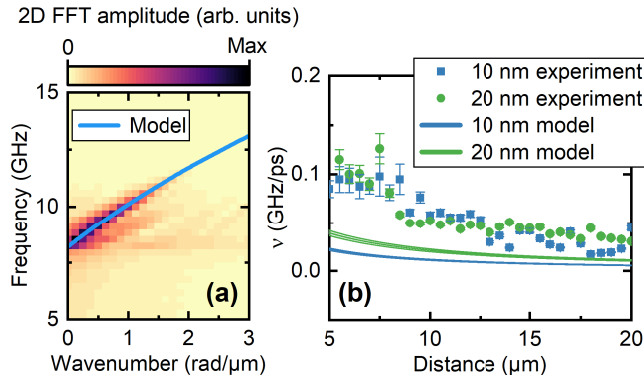


FIG. 3. (a) Dispersion of MSSW wave packet in 20-nm iron film in HA-configuration, reconstructed from experimental time-space maps (pseudo-color) and calculated analytically with Eq. (2) (line). (b) Chirp parameter ν versus distance for 10 and 20 nm films in HA-configuration. Symbols show experimental data, lines – analytical calculations with Eq. (3) with $T_0 = 50$ ps.

with broadband spectra is needed, but it is out the scope of this letter. Importantly, the value of ν depends on d and F . The dependence on F means that the resulting chirp of MSSW wave packets is programmable with the intrinsic effective field of the waveguide, e.g., its saturation magnetization, anisotropy parameters, dimensions etc. Notably, the chirp of the MSSWs in iron films reported here has been clearly seen in previous experiments with micro-stripe antennae⁹, but it was not discussed yet.

In conclusion, we show experimentally the propagation of optically excited MSSWs in thin iron films with propagation distances of order tens of microns, which may find the application in magnonic waveguides and logic gates. Additional advantages of iron as a metal for magnonic applications include the relatively easy manufacturing procedure of the thin films and the strong in-plane magneto-crystalline anisotropy. We use the latter here to tune the character of the MSSW wave packet spectrum evolution in the presence of laser-induced thermal gradients and its chirping with distance. Generated wave packets are spectrally broad and hardly to describe analytically. Nonetheless, the analysis of optically generated ultra broadband SW packets is crucial for wave-based data processing in future hybrid magnonic-photonic devices. Furthermore, the optical pump-probe technique gives a powerful toolbox for the detailed investigation of the SWs packet including: the extraction of its spectral

evolution in space, the dispersion law, and the chirping in the time domain. The first two options are available with Brillouin light scattering (BLS) techniques as well^{36,37}, while the chirping investigation is accessible in BLS with introduction phase resolution with corresponding complication of the measurement scheme³⁸, or, alternatively, with the scanning antennae technique^{39,40}. The ultrafast laser pulses provide all above possibilities out-of-box with excellent spatial and temporal resolution.

ACKNOWLEDGMENTS

The work of Ia.A.F. and P.I.G. was funded by RFBR (grant 20-32-70149), A.M.K. acknowledges RSF (grant 20-12-00309), N.E.Kh. acknowledges the "BASIS" Foundation (grant 19-1-3-42-1).

AUTHOR DECLARATIONS

Conflict of Interest

The authors have no conflicts to disclose.

DATA AVAILABILITY

The data that support the findings of this study are available from the corresponding author upon reasonable request.

- ¹P. Pirro, V. I. Vasyuchka, A. A. Serga, and B. Hillebrands, *Nat Rev Mater* **1666** (2021), 10.1038/s41578-021-00332-w.
- ²A. Yamaguchi, A. Hirohata, and B. J. Stadler, eds., "Chapter 5 - spintronics," in *Nanomagnetic Materials*, Micro and Nano Technologies (Elsevier, 2021) pp. 305–424.
- ³S. A. Nikitov, D. V. Kalyabin, I. V. Lisenkov, A. N. Slavin, Y. N. Barabanenkov, S. A. Osokin, A. V. Sadovnikov, E. N. Beginin, M. A. Morozova, Y. P. Sharaevsky, Y. A. Filimonov, Y. V. Khivintsev, S. L. Vysotsky, V. K. Sakharov, and E. S. Pavlov, *Phys. Usp.* **58**, 1002 (2015).
- ⁴A. Mahmoud, F. Ciubotaru, F. Vanderveken, A. V. Chumak, S. Hamdioui, C. Adelman, and S. Cotofana, *Journal of Applied Physics* **128**, 161101 (2020).
- ⁵A. Barman, G. Gubbiotti, S. Ladak, A. O. Adeyeye, M. Krawczyk, J. Gräfe, C. Adelman, S. Cotofana, A. Naeemi, V. I. Vasyuchka, B. Hillebrands, S. A. Nikitov, H. Yu, D. Grundler, A. V. Sadovnikov, A. A. Grachev, S. E. Sheshukova, J.-Y. Duquesne, M. Marangolo, G. Csaba, W. Porod, V. E. Demidov, S. Urazhdin, S. O. Demokritov, E. Albisetti, D. Petti, R. Bertacco, H. Schultheiss, V. V. Kruglyak, V. D. Poimanov, S. Sahoo, J. Sinha, H. Yang, M. Münzenberg, T. Moriyama,

- S. Mizukami, P. Landeros, R. A. Gallardo, G. Carlotti, J.-V. Kim, R. L. Stamps, R. E. Camley, B. Rana, Y. Otani, W. Yu, T. Yu, G. E. W. Bauer, C. Back, G. S. Uhrig, O. V. Dobrovolskiy, B. Budinska, H. Qin, S. van Dijken, A. V. Chumak, A. Khitun, D. E. Nikonov, I. A. Young, B. W. Zingsem, and M. Winklhofer, **33**, 413001 (2021).
- ⁶A. Khitun, M. Bao, and K. L. Wang, *Journal of Physics D: Applied Physics* **43**, 264005 (2010).
- ⁷G. Csaba, Á. Papp, and W. Porod, *Physics Letters A* **381**, 1471 (2017).
- ⁸Y. Khivintsev, A. Kozhevnikov, G. Dudko, V. Sakharov, Y. Filimonov, and A. Khitun, *Physics of Metals and Metallography* **120**, 1318 (2019).
- ⁹K. Sekiguchi, S.-W. Lee, H. Sukegawa, N. Sato, S.-H. Oh, R. D. McMichael, and K.-J. Lee, *NPG Asia materials* **9**, e392 (2017).
- ¹⁰N. E. Khokhlov, P. I. Gerevenkov, L. A. Shelukhin, A. V. Azovtsev, N. A. Pertsev, M. Wang, A. W. Rushforth, A. V. Scherbakov, and A. M. Kalashnikova, *Phys. Rev. Appl.* **12**, 044044 (2019).
- ¹¹A. Kozhevnikov, F. Gertz, G. Dudko, Y. Filimonov, and A. Khitun, *Applied Physics Letters* **106**, 142409 (2015).
- ¹²E. Albisetti, S. Tacchi, R. Silvani, G. Scaramuzzi, S. Finizio, S. Wintz, C. Rinaldi, M. Cantoni, J. Raabe, G. Carlotti, R. Bertacco, E. Riedo, and D. Petti, *Advanced Materials* **32**, 1906439.
- ¹³T. Satoh, Y. Terui, R. Moriya, B. A. Ivanov, K. Ando, E. Saitoh, T. Shimura, and K. Kuroda, *Nature Photonics* **6**, 662– (2012).
- ¹⁴A. I. Chernov, M. A. Kozhaev, A. Khramova, A. N. Shaposhnikov, A. R. Prokopov, V. N. Berzhansky, A. K. Zvezdin, and V. I. Belotelov, *Photon. Res.* **6**, 1079 (2018).
- ¹⁵I. Yoshimine, Y. Y. Tanaka, T. Shimura, and T. Satoh, **117**, 67001 (2017).
- ¹⁶T. Hioki, Y. Hashimoto, and E. Saitoh, *Commun Phys* **3**, 188 (2020).
- ¹⁷Y. Au, M. Dvornik, T. Davison, E. Ahmad, P. S. Keatley, A. Vansteenkiste, B. Van Waeyenberge, and V. V. Kruglyak, *Phys. Rev. Lett.* **110**, 097201 (2013).
- ¹⁸N. Khokhlov, A. Khramova, I. Filatov, P. Gerevenkov, B. Klinskaya, and A. Kalashnikova, *Journal of Magnetism and Magnetic Materials* **534**, 168018 (2021).
- ¹⁹M. Gester, C. Daboo, R. J. Hicken, S. J. Gray, A. Ercole, and J. A. C. Bland, *Journal of Applied Physics* **80**, 347 (1996).
- ²⁰G. Wastlbauer and J. A. C. Bland*, *Advances in physics* **54**, 137 (2005).
- ²¹D. Parkes, L. Shelford, P. Wadley, V. Holý, M. Wang, A. Hindmarch, G. Van Der Laan, R. Campion, K. Edmonds, S. Cavill, *et al.*, *Scientific reports* **3**, 1 (2013).
- ²²I. A. Filatov, P. I. Gerevenkov, M. Wang, A. W. Rushforth, A. M. Kalashnikova, and N. E. Khokhlov, *J. Phys.: Conf. Ser.* **1697**, 012193 (2020).
- ²³A. Chumak, A. Serga, and B. Hillebrands, *Journal of Physics D: Applied Physics* **50**, 244001 (2017).
- ²⁴P. Gerevenkov, D. Kuntu, I. A. Filatov, L. Shelukhin, M. Wang, D. Pattnaik, A. Rushforth, A. Kalashnikova, and N. Khokhlov, *Physical Review Materials* **5**, 094407 (2021).
- ²⁵A. Gurevich and G. Melkov, *Magnetization Oscillations and Waves* (Taylor & Francis, 1996).
- ²⁶B. A. Kalinikos, M. P. Kostylev, N. V. Kozhus, and A. N. Slavin, *J. Phys.: Condens. Matter* **2**, 9861 (1990).
- ²⁷M. Jäckl, V. I. Belotelov, I. A. Akimov, I. V. Savochkin, D. R. Yakovlev, A. K. Zvezdin, and M. Bayer, *Phys. Rev. X* **7**, 021009 (2017).
- ²⁸T. Dehoux and B. Audoin, *Journal of Applied Physics* **112**, 124702 (2012).
- ²⁹M. Danworaphong, M. Tomoda, Y. Matsumoto, O. Matsuda, T. Ohashi, H. Watanabe, M. Nagayama, K. Gohara, P. H. Otsubuka, and O. B. Wright, *Applied physics letters* **106**, 163701 (2015).
- ³⁰D. Marcuse, *Appl. Opt.* **19**, 1653 (1980).
- ³¹S. A. Akhmanov, V. A. Vysloukh, and A. S. Chirkin, *Usp. Fiz. Nauk* **149**, 449 (1986).
- ³²G. P. Agrawal, *Nonlinear Fiber Optics*, 6th ed. (Academic Press, 2019).
- ³³A. K. Zvezdin and A. F. Popkov, *JETP* **57**, 350 (1983).
- ³⁴R. Arias and D. L. Mills, *Phys. Rev. B* **60**, 7395 (1999).
- ³⁵K. Zakeri, *J. Phys.: Condens. Matter* **32**, 363001 (2020).
- ³⁶S. Demokritov, B. Hillebrands, and A. Slavin, *Physics Reports* **348**, 441 (2001).
- ³⁷D. V. Kalyabin, A. V. Sadovnikov, E. N. Beginin, and S. A. Nikitov, *Journal of Applied Physics* **126**, 173907 (2019).
- ³⁸F. Fohr, A. Serga, T. Schneider, J. Hamrle, and B. Hillebrands, *Review of Scientific Instruments* **80**, 043903 (2009).
- ³⁹A. Y. Annenkov, S. V. Gerus, and E. H. Lock, *EPL* **123**, 44003 (2018).
- ⁴⁰A. Y. Annenkov and S. V. Gerus, *J. Commun. Technol. Electron.* **57**, 519 (2012).